optica

Quantitative fluorescence correlation spectroscopy in three-dimensional systems under stimulated emission depletion conditions

KRZYSZTOF SOZANSKI,[1,3] EVANGELOS SISAMAKIS,[2] XUZHU ZHANG,[1] AND ROBERT HOLYST[1,4]

[1]Institute of Physical Chemistry, Polish Academy of Sciences, Kasprzaka 44/52, 01-224 Warsaw, Poland
[2]PicoQuant GmbH, Rudower Chaussee 29, 12489 Berlin, Germany
[3]e-mail: ksozanski@ichf.edu.pl
[4]e-mail: rholyst@ichf.edu.pl

Received 17 April 2017; revised 14 July 2017; accepted 16 July 2017 (Doc. ID 292984); published 11 August 2017

Superresolution fluorescence microscopy is becoming a widely available, standard tool in biophysical research. The leading deterministic approach, stimulated emission depletion (STED), can enhance the capabilities of various fluorescence techniques, including fluorescence correlation spectroscopy (FCS). Until now, STED-FCS has been successfully applied to diffusion studies in 2D systems such as membranes. Severe deficiencies, including overestimation of the detected number of probes as well as underestimation of their diffusion coefficients (both parameters differing from the expected values by up to an order of magnitude) impeded STED-FCS studies in solutions. Here, we introduce a realistic 3D model of the detection volume for STED-FCS and use it to resolve the apparent inconsistencies. To validate the model, we show a range of STED-FCS experimental data on free diffusion of probes in solutions, covering a broad range of diffusion coefficients and STED power levels. We define the limitations of STED-FCS in 3D and provide simple guidelines for experiment design and data analysis. The proposed approach should prove useful for particle mobility and reaction kinetics studies in polymer solutions as well as in bulk biomimetic and biological systems, especially when reactant concentrations exceeding 100 nM are required.

OCIS codes: (170.2520) Fluorescence microscopy; (100.6640) Superresolution; (290.1990) Diffusion.

https://doi.org/10.1364/OPTICA.4.000982

1. INTRODUCTION

According to the diffraction limit, a wave cannot be focused to a spot narrower than its wavelength λ divided by double the numerical aperture of the lens. This restricts the resolution of optical microscopes to about 200 nm. However, superresolution techniques [1] allow us to circumvent this limitation, offering resolution of the order of 20 nm [2–6] or even below 10 nm [7]. A particularly successful approach is stimulated emission depletion (STED) microscopy [8,9]. STED employs a depleting laser, coaxial to the excitation beam and featuring a zero-intensity center (a so-called donut). It disables spontaneous fluorescence at the periphery of the detection spot, trimming it to subdiffraction size [10]. A combination of STED with fluorescence correlation spectroscopy (FCS) opens a perspective of molecular mobility and chemical kinetics studies at the nanometer-length scale [11]. Numerous successful STED-FCS investigations of 2D systems (membranes) have been reported [12–15]. However, similar studies in solutions are scarce [11,16,17] and raise some concerns: diffusion times are only moderately shortened (the change is lower by even an order of magnitude than expected on the basis of 2D experiments), the apparent number of molecules increases with the shrinking detection volume, and the signal-to-noise ratio is surprisingly low. Hereby, we explain these observations, provide simple guidelines for data analysis, and define the limitations of the method. Our approach is based on a realistic description of the 3D detection volume upon STED. We propose a model for analysis of autocorrelation that allows us to account for the intrinsic noise and provides a robust measure of the effective length scale at which diffusion is observed. We demonstrate the validity of the methodology in a series of STED-FCS experiments, covering a range of probe radii (0.7–6.9 nm) and various medium compositions [addition of low molecular weight polyethylene glycol (PEG) changes both the viscosity and the refractive index of the sample with no viscosity scaling effects [18]].

In FCS, fluorescence originating from the detection volume is recorded. An autocorrelation function $G(\tau)$ is used to elucidate temporal patterns from the fluorescence intensity fluctuations [19,20], which correspond to the time spent by the probes in the detection volume. This volume is not a geometric shape with sharp edges but rather a continuous function $p(\mathbf{r})$ describing the probability of detecting a photon originating from a given point $\mathbf{r}$ [21]. For the 3D Gaussian $p_{conf}(\mathbf{r})$, usually assumed for confocal optics, an analytical expression for $G(\tau)$ can be produced, which is fitted to the experimental autocorrelation curve to yield the

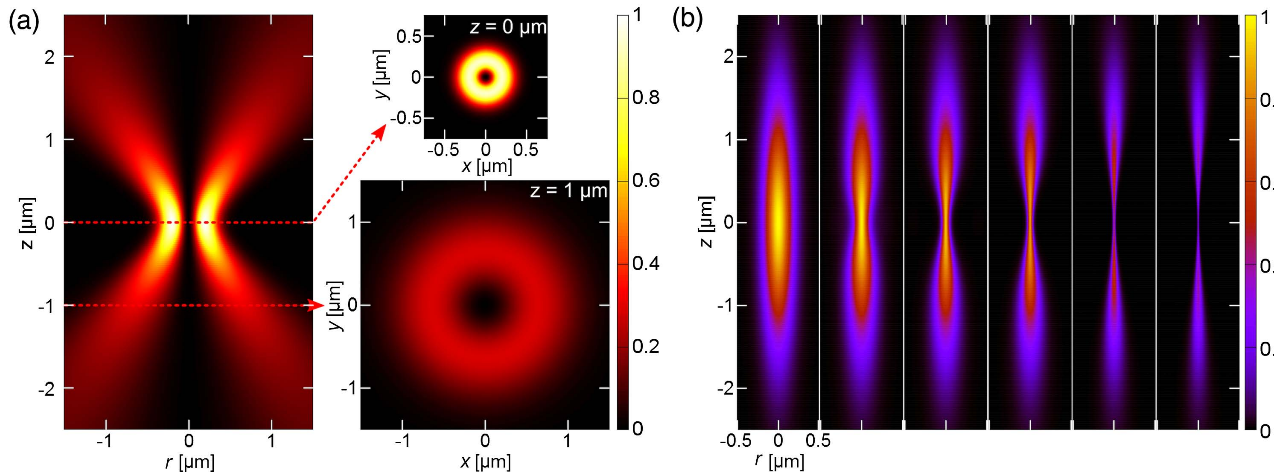

Fig. 1. (a) STED depletion pattern p_{STED} according to Eq. (5): vertical and horizontal sections (at the focal plane and 1 μm away from it). (b) STED-FCS detection profiles p_{eff} for $P_{\mathrm{STED}} = 0, 0.1, 0.5, 1, 5, 10\, P_{\mathrm{sat}}$ (left to right) according to Eq. (6), normalized to the maximum of the $P_{\mathrm{STED}} = 0$ case. Decrease in $p_{\mathrm{eff}}(0, 0)$ with increasing STED is due to nonperfect zero in the depletion pattern [29]; for details, see Section S5 of Supplement 1.

diffusion time τ_D and number of the probes N in the detection volume [for a detailed introduction to FCS and related TCSPC methods, see, e.g., [20,22] and a short summary in Section 1 of Supplement 1]. For free diffusion in three dimensions, τ_D depends on the diffusion coefficient of the probe D as

$$\tau_D = \omega^2/4D, \tag{1}$$

where ω is the radius [23] of $p_{\mathrm{conf}}(\mathbf{r})$. In the simplest case, when only translational diffusion is considered, N is calculated as $1/G(0)$, i.e., reciprocal of the amplitude of the autocorrelation function. However, $G(\tau)$ it is dampened by uncorrelated noise. This effect can be accounted for by including a correction for the signal-to-noise ratio SNR, which gives [24,25]

$$N = \frac{1}{(1 + 1/\mathrm{SNR})^2} \frac{1}{G(0)}. \tag{2}$$

Accurate determination of SNR as well as the dimensions and shape of the detection volume are essential for proper analysis of autocorrelation data. Several ideas on how to resolve these issues in case of application of STED to 3D systems have already been proposed. Both fluorescence intensity distribution analysis (FIDA) [16,26] and stimulated emission double depletion (STEDD) [27] offer experimental estimations of correction factors to account for noncorrelating backgrounds. An emerging approach called separation of photons by lifetime tuning (SPLIT) [17] features the application of advanced fluorescence lifetime filters to the data to limit the background contribution. Despite the applicability of these methods, none of them provides a detailed, physically accurate description of the effective detection profile in STED-FCS. This in turn is necessary to pinpoint the source of the background increase, predict the SNR values, explain the modest decrease in diffusion times upon application of STED, as well as determine and justify the limitations of the method. In this contribution, we provide such basis for STED-FCS in solutions, supporting our theoretical arguments with experimental STED-FCS results and providing simple, ready-to-use procedures for data analysis.

2. MATERIALS AND METHODS

STED-FCS experiments were performed with a MicroTime 200 (PicoQuant) time-resolved fluorescence microscope with a STED add-on and a 100×/1.4 oil immersion objective (Olympus M Plan Apochromat). The system featured the *easySTED* phase plate set [28] to form the depleting beam into a donut of intensity in the center of around 1% of the maximum value [29], while the excitation beam remained unaffected. Both excitation and depletion lasers (LDH-640 and VisIR 765 "STED" [30], PicoQuant) were operated in pulsed mode. The gated STED approach was adopted [15,31,32], wherein a nanosecond-range gating was used to filter photon counts and limit the contribution of photons originating from outside of the donut center (for details, see, e.g., [33]) and bleed-through of stimulated emission. A STED pulse was introduced for every other excitation pulse, so that intrinsic, on-line non-STED control was recorded during every experiment in a pulsed interleaved way [15] (for details, see Section S2 of Supplement 1). Atto 647N dye and its conjugates were used in STED-FCS, which practically excluded direct excitation of fluorophores with the STED laser (cf. Fig. S2 for UV–Vis spectra).

Atto dyes were purchased from AttoTec GmbH, 20 nm crimson fluorescent microspheres were obtained from Thermo Fisher Scientific, and bovine serum albumin (BSA), apoferritin, and PEG 400 Da came from Sigma. Protein labeling and purification was performed according to the manufacturer's protocol. Measurements were done in a #1 8-well Nunc Lab-Tek chambered coverglass. For FCS simulations, SimFCS 4 (Laboratory for Fluorescence Dynamics, UC at Irvine, California, USA) was used. Further experimental details can be found in Section S4 of Supplement 1.

3. RESULTS AND DISCUSSION

A. Illumination, Depletion, and Detection Profiles

It is assumed in confocal microscopy that the radial distribution of the excitation beam intensity is Gaussian. The width of the beam w changes with z position as

$$w(z) = w_0\sqrt{1+\left(\frac{z}{z_R}\right)^2}, \quad (3)$$

where z_R is the Rayleigh length (defined as $z_R = \pi w_0^2/\lambda$) and w_0 is the beam waist. Confocal pinhole, introduced in the detection path, trims the observed volume to an elongated ellipsoid. The resulting detection profile is a 3D Gaussian, $p_{\text{conf}}(\mathbf{r}) = \exp(-2r/\omega_{\text{conf}}^2)\exp(-2z/z_{\text{conf}}^2)$, with axial dimension of z_{conf} and radius $\omega_{\text{conf}} = w_0$ independent of z (visualizations available in Section S5 of Supplement 1).

Probability of stimulated emission depends exponentially on STED intensity [34]. Effective radius of the detection spot ω_{eff} is expected to change with STED power P_{STED} as [2,5]

$$\omega_{\text{eff}} = \frac{\omega_{\text{conf}}}{\sqrt{1+P_{\text{STED}}/P_{\text{sat}}}}. \quad (4)$$

Saturation power P_{sat} is defined as such P_{STED} that the overall intensity of spontaneous fluorescence is decreased by half [2,5].

The radial profile of the STED beam is well described by a first-order Laguerre–Gaussian function [35,36]. However, the analogy to confocal detection volume [36] cannot be applied to the STED profile in the axial dimension since the STED beam itself is not affected by the pinhole. Instead, a z-dependent normalization factor should be included to account for the off-focus broadening of $w_{\text{STED}}(z)$ [by analogy to Eq. (3)] that would maintain the condition of constant photon flux across every plane (i.e., the same value of $\int p_{\text{STED}}(\mathbf{r})\mathrm{d}r$ for every z). We propose to describe the depleting beam, visualized in Fig. 1(a), as

$$p_{\text{STED}}(\mathbf{r}) = \frac{1}{\sqrt{1+\frac{z}{z_R}}}\left(\frac{r}{w_{\text{STED}}(z)}\right)^2\exp\left(\frac{-2r^2}{w_{\text{STED}}^2(z)}\right). \quad (5)$$

In further calculations, we also include a correction for the nonperfect zero in the $p_{\text{STED}}(\mathbf{r})$ depletion pattern [29]; for details, see Section S5 of Supplement 1. To obtain the effective detection profile p_{eff}, we must overlay the confocal detection p_{conf} with the depleting beam p_{STED}, including the nonlinear dependence of the depletion efficiency on STED intensity [34]:

$$p_{\text{eff}}(\mathbf{r}) = p_{\text{conf}}(\mathbf{r})\exp(-a p_{\text{STED}}(\mathbf{r})), \quad (6)$$

where a is a dimensionless parameter describing the STED intensity. Total fluorescence intensity corresponds to the integral of $p_{\text{eff}}(\mathbf{r})$ over the whole space. For any given z position, $p_{\text{eff}}(r)$ retains a Gaussian-like shape. However, its width ω_{eff} is a function of z and $p_{\text{eff}}(z)$ is not Gaussian.

We modeled our experimental system with Eq. (6). To provide the input parameters, we performed separate FCS experiments with Atto 674N diffusing in PBS, which yielded the confocal detection volume radius $\omega_{\text{conf}} = 237$ nm and aspect ratio $z_{\text{conf}}/\omega_{\text{conf}} = 8.0$. We assumed the depleting beam to be broader than the excitation beam by a factor of 1.184 due to its longer wavelength, giving $w_{\text{STED}}(z=0) = 281$ nm and $z_R = 323$ nm. Using these values and the numerical integration of Eq. (6), we found that P_{sat} corresponds to $a = 88$. Evolution of p_{eff} with increasing STED intensity is shown in Fig. 1(b).

Depletion is most effective in the focal plane ($z = 0$), causing a rapid drop in $\omega_{\text{eff}}(z=0)$ upon STED. However, broader detection lobes remain in the out-of-focus areas. This significantly influences the SNR and τ_D values.

B. Signal-To-Noise Ratio

Detection volume in FCS is usually interpreted as the area where the normalized value of $p_{\text{conf}}(\mathbf{r})$ is above $1/e^2$ [20]. Only fluorescence originating from this area, strongly contributing to the autocorrelation, should be treated as signal. Molecules in the dim fringe regions are less likely to contribute to autocorrelation. Therefore, fluorescence coming from those areas contributes to noise rather than signal. On this basis, we introduce an idealized definition of SNR, where signal is fluorescence originating from within the $1/e^2$ boundary and noise is fluorescence from the dim outer region. This definition excludes any background, such as stray photons, detector dark counts, etc. For confocal FCS, such an SNR value is the ratio of integrals of $p_{\text{conf}}(\mathbf{r})$ calculated over the detection volume and its complement. This gives SNR = 10.2. We performed analogous calculations for the STED detection volume [described by Eq. (6)], taking $\omega_{\text{eff}}(0)$ and z_{conf} as arbitrary detection volume limits. The result is presented in Fig. 2. SNR decreases quickly with P_{STED}. Utilizing Eq. (2), we can estimate the influence of this effect on $G(0)$ and include appropriate correction for N. The inset in Fig. 2 demonstrates the validity of such approach on the example of BSA diffusion. N taken directly from $G(0)$ remains nearly constant at low STED and then counterintuitively increases. Including the SNR correction grants monotonic decrease of $N(P_{\text{STED}})$. The corrected experimental N values match those calculated on the basis of the expected detection volume changes.

C. Autocorrelation Fitting and Interpretation

Implementing the $p_{\text{eff}}(\mathbf{r})$ profile in the autocorrelation integrals renders it impossible to provide an analytical form of the autocorrelation equation. Thus, there is no full yet practical $G(\tau)$ model for STED-FCS. To overcome this issue, we propose the following approximation featuring a simple 2D model:

$$G(\tau) = G(0)\left(1+\frac{\tau}{\tau_D}\right)^{-1}. \quad (7)$$

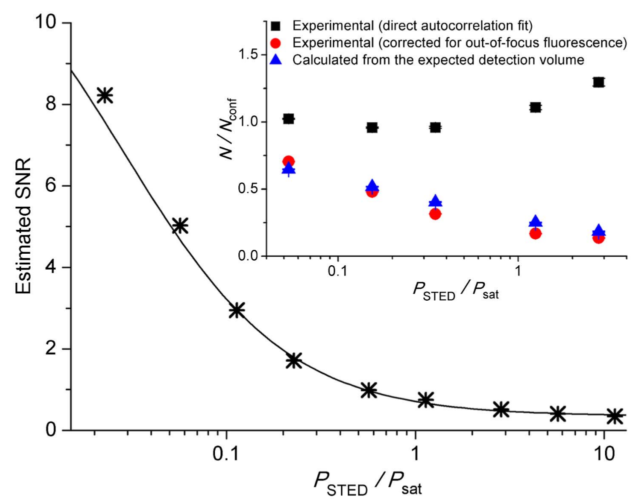

Fig. 2. Decrease of SNR with increasing P_{STED} according to the proposed model. The inset shows changes in the apparent number N of BSA molecules in the detection volume upon increasing STED power (experimental data, scaled by N_{conf} corresponding to $P_{\text{STED}} = 0$). Squares represent data obtained directly from autocorrelation fitting, circles are the same data corrected for SNR via Eq. (2), and triangles are values calculated on the basis of the expected detection volume decrease.

Due to elongation of the detection volume, diffusion in the axial direction only marginally contributes to autocorrelation (see Section S6 of Supplement 1 for a broader discussion). $p_{\mathrm{eff}}(r)$ is Gaussian in every horizontal plane. The simple form of Eq. (7) limits the number of parameters to two and provides reasonable fits of experimental STED-FCS autocorrelation curves.

To calculate D from fitted τ_D values, the characteristic dimension of the detection volume ω is needed [cf. Eq. (1)]. However, in STED-FCS, ω_{eff} is a function of z. Also, the focal plane is not the brightest (i.e., producing most photons) section of the detection volume. Although $p_{\mathrm{eff}}(\mathbf{r})$ takes its maximum at $\mathbf{r} = (0, 0)$, $\omega_{\mathrm{eff}}(z)$ has a minimum at $z = 0$. Integrating $p_{\mathrm{eff}}(\mathbf{r})$ over r for given z allows us to assess the contribution of each plane to the overall fluorescence. A range of calculation results for various STED intensities is presented in Fig. 3. For instance, at $P_{\mathrm{STED}} = P_{\mathrm{sat}}$ the brightest regions are symmetrically located around $z = 0.8$ and $z = -0.8$ µm, where ω_{eff} reaches 150 nm (compared to ~40 nm at $z = 0$). For any given P_{STED} value such brightest sections can be found. We propose to use the value of ω_{eff} corresponding to these brightest sections, denoted further as ω_{app}, as the apparent characteristic dimension of the detection volume in STED-FCS data analysis. For $P_{\mathrm{STED}} = 0$, ω_{app} reduces to ω_{conf}, which is independent of z. However, the higher the STED intensity, the greater the discrepancy between ω_{app} and $\omega_{\mathrm{eff}}(z = 0)$, as depicted in Fig. 4. This discrepancy is the reason why the decrease of τ_D in STED-FCS in solutions is much less pronounced than in the case of 2D systems, where only the $\omega_{\mathrm{eff}}(z = 0)$ value is of importance.

D. STED-FCS Experimental Results

To validate the proposed model, we performed a range of STED-FCS experiments for probes freely diffusing in solutions. As probes, we used free Atto 647N dye as well as proteins—bovine serum albumin (BSA) and apoferritin—labeled with this dye. To achieve a broad range of diffusion rates, we used PEG (average molecular weight 400 Da, concentrations up to 40%)

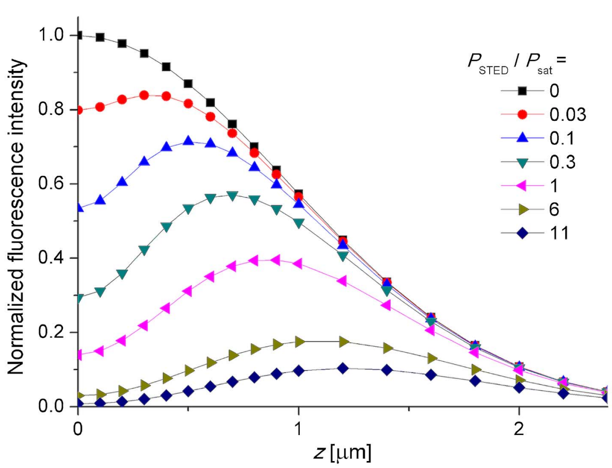

Fig. 3. Intensity of fluorescence originating from different horizontal sections of the detection volume at various STED intensities according to the proposed model. Due to the most effective depletion in the vicinity of the focal plane, the brightest regions of the detection volume are located in the off-focus lobes rather than at $z = 0$. The plotted datapoints were calculated as integrals of $p_{\mathrm{STED}}(\mathbf{r})$ over r for a given z coordinate and normalized to the non-STED maximum value.

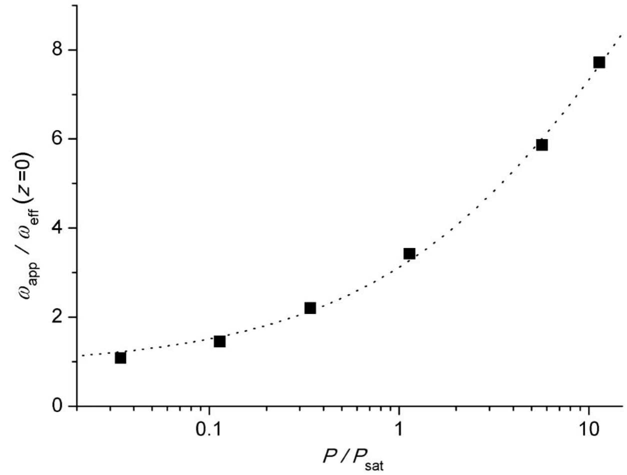

Fig. 4. Dependence of the ratio of the apparent STED-FCS detection radius ω_{app} (i.e., ω_{eff} of the brightest z section) to ω_{eff} at the focal plane on the STED power, calculated according to the proposed detection profile description. The higher the STED intensity, the greater the discrepancy between the apparent radius of the 3D detection volume and its radius at the beam waist (in the focus plane).

to slow down the probe motion in selected experiments. In Fig. 5, we plot exemplary, representative autocorrelation data recorded for Atto 647N in PBS and BSA in 20% PEG. The fitted curves correspond to the standard 3D, free diffusion autocorrelation model [see Supplement 1, Eq. (S2)] for the confocal case and the model disregarding axial diffusion for the STED case [Eq. (7)].

All the STED-FCS experimental results obtained for different probe/medium systems and STED powers are collected in Fig. 6. To enable direct comparison between different systems, τ_D is scaled in all cases by τ_{conf}, i.e., the diffusion time for a given probe in a given medium at $P_{\mathrm{STED}} = 0$. Since susceptibility of fluorophores to stimulated emission depends on their environment [5,13], STED power values are scaled by saturation power. P_{sat} for every sample was retrieved separately. This was done by finding the P_{STED} value at which total fluorescence decreased by 50%, simply interpolating the total spontaneous fluorescence intensity recorded for a given sample at various P_{STED} values. P_{sat} ranged from 8 to 27 mW. Plotting diffusion times as a function of the $P_{\mathrm{STED}}/P_{\mathrm{sat}}$ ratio allows us to account for these differences. It is important to note that this point is neglected in the common STED-FCS experimental scheme, where either a series of FCS measurements in a reference solution of a probe of known D or scanning of immobilized beads is performed at various P_{STED} and the obtained ω_{eff} values are directly applied to the data acquired from the sample.

The empty squares and solid line overlaid over the experimental data in Fig. 6 correspond to the relative diffusion times expected from the detection volume model proposed in this paper. Importantly, the model includes no fitted parameters. It provides a reasonable description of the data, even though it assumes no optical aberrations, a perfectly round donut (which in reality is somewhat square-like in the *easySTED* approach), and a simple approximation of $G(\tau)$. Clearly, the postulated description is more relevant than the standard approach, which neglects the STED-dependent changes in the axial profile of

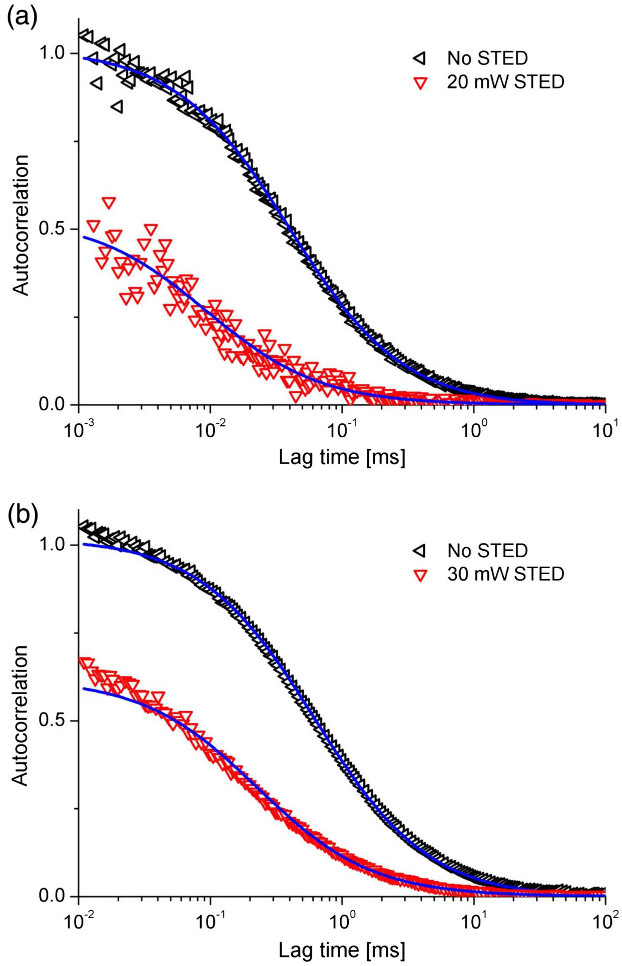

Fig. 5. Exemplary experimental autocorrelation curves for (a) Atto 647N in PBS and (b) BSA in 20% PEG. In both cases, representative data for an intermediate STED power and confocal (non-STED) reference are plotted. Blue curves represent fits according to Eq. (7). Both plots are normalized to the fitted amplitude of the confocal FCS case.

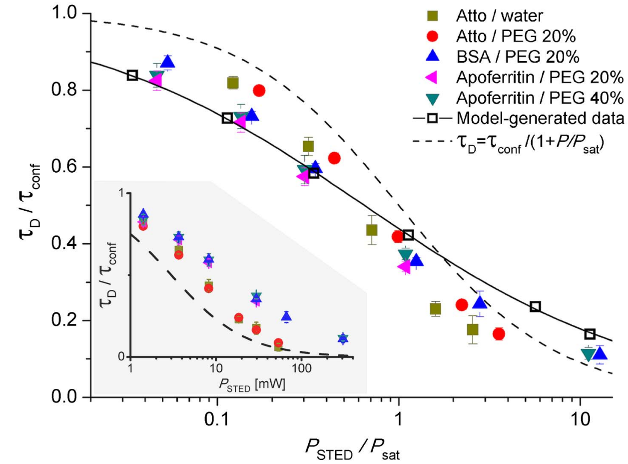

Fig. 6. Diffusion times τ_D (scaled by the non-STED values τ_{conf}) measured for various probes and environments. STED power P_{STED} is scaled by the saturation power P_{sat}, established individually for each sample. The empty squares and solid line correspond to the model presented hereby (no fitted parameters). Since in all cases only normal free diffusion is expected, it is assumed that D is independent from the length scale of observation. The dashed line represents the simplistic approach of Eq. (4). For comparison, in the shaded inset, the same data are plotted directly against P_{STED} values, along with Eq. (4) including $P_{sat} = 3.0$ mW from bead scanning (standard calibration procedure) and disregarding the changes in the axial profile of the detection volume upon STED.

the detection volume and utilizes calibration based on probe scanning (inset in Fig. 6).

STED-FCS results are comparable with simplistic predictions based on Eqs. (1) and (4). More accurate estimation of τ_D is provided by the detection-volume-based model proposed hereby. A crucial condition in all cases is that P_{sat} is individually established for a given sample. Even assuming no change in the fluorophore properties, P_{sat} in a 3D system is ~7 times greater than in a membrane (due to less effective depletion away from the focal plane). A recommendable experimental practice is to perform calibration on a simple system (e.g., dye in solution) to establish the dependence of τ_D/τ_{conf} on P_{STED}/P_{sat}. The decrease of τ_D with the P_{STED}/P_{sat} ratio is closely comparable for different probes.

E. Reference Simulations and Experiments

In 2D imaging of immobilized 20 nm beads we reached a 10-fold decrease in the detection spot radius upon STED (cf. Fig. S7). However, the limit of τ_D/τ_{conf} in STED-FCS was around 0.1, which corresponded to just a three-fold decrease in the effective detection spot radius. We initially suspected that, due to shortened τ_D, probes did not produce correlatable photon pairs during their brief residence in the detection volume. To verify whether the autocorrelation function itself is prone to systematic errors at extremely short diffusion times and counts per molecule passage, we performed simulated FCS runs for a range of subdiffraction detection volumes. We used the SimFCS software, wherein random motion of fluorophores over a grid was simulated, with a predefined 3D Gaussian detection profile placed centrally in the simulation box. On the basis of time traces generated in such manner, autocorrelation curves were calculated and fitted with the free 3D diffusion model. For all simulations, D was set to 200 $\mu m^2/s$, molecular brightness to 25,000 counts per second, and axial dimension of the detection volume to 2 μm to mimic the conditions of real experiments.

In Fig. 7, we depict the changes in the apparent number of probes N with the radius of the simulated all-Gaussian detection volume. We compare the values calculated on the basis of the set detection volume, extracted from the amplitude of the obtained autocorrelation curves, computed from the fitted diffusion times, and estimated on the basis of changes in the count rate. In the case of no added background [Fig. 7(a)], all these values are perfectly congruent. This implies that even for extremely short diffusion times (of the order of a single microsecond) and a relatively dim probe, the autocorrelation is not distorted. Results of simulations including background [Fig. 7(b)], where the amount of added random counts was set to match the estimation depicted in Fig. 2, are given in Fig. 7(b). For the smallest detection volumes, the apparent N extracted from the autocorrelation amplitude was heavily overestimated [as expected from Eq. (2)], which was also the case for the count-rate-based estimates. However, the values retrieved from fitted diffusion times still followed the $N \propto V \propto \omega^2$ dependence. While the decrease of the SNR did

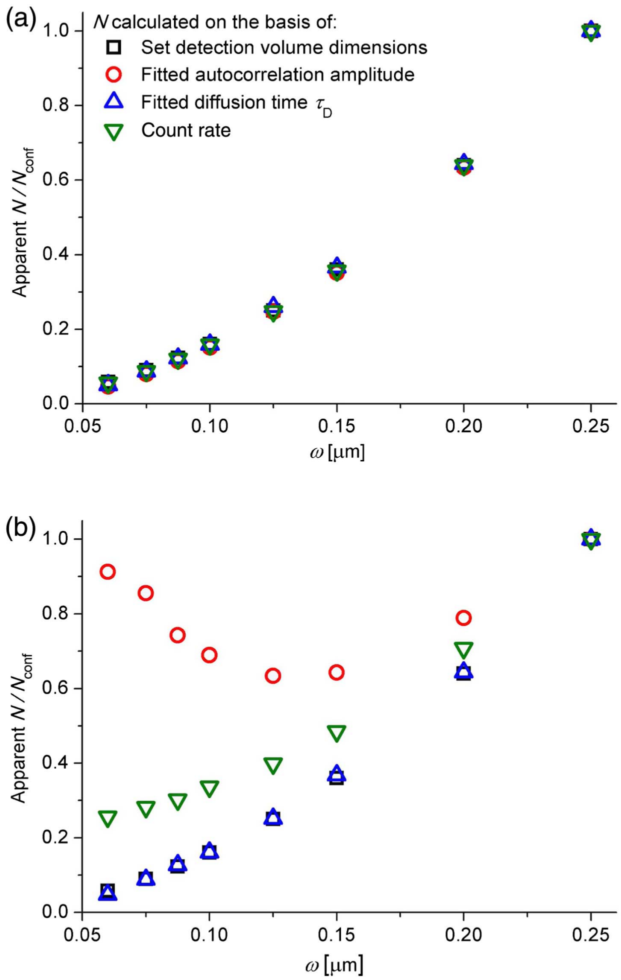

Fig. 7. Results of FCS simulations: apparent number of molecules N scaled by N_{conf} (i.e., number of molecules in a diffraction-limited detection volume radius of $\omega_{\mathrm{conf}} = 0.25\ \mu\mathrm{m}$) calculated on the basis of various parameters obtained from single simulation runs. (a) No added background. (b) Random background counts added to the raw time trace. Legend refers to both panels.

contribute to the autocorrelation amplitude dampening, it did not influence the recorded τ_D values.

Thus, the simulation results suggest that the diffusion times observed in STED-FCS should not be burdened with any artifacts related to the short time of passage through the detection volume and low number of photon counts per event. To further support such conclusions, we performed additional, independent confocal FCS experiments at low excitation power. The values of τ_D obtained from autocorrelation fitting were correct even at less than 0.1 photon counts per molecule per τ_D, while the amplitude offset was triggered by low SNR (for details, see Section S8 of Supplement 1). Also, the $\tau_D/\tau_{\mathrm{conf}}$ limit observed in our STED-FCS experiments was similar for Atto 647N in water and apoferritin in 40% PEG, despite a 20-fold difference in τ_D between these two cases. All the above observations allow us to claim that changes in τ_D observed in STED-FCS indeed stem from the shifts in the shape of the detection profile upon application of STED [Eqs. (5) and (6)] and are not afflicted by experimental artifacts.

4. CONCLUSIONS

Implementation of STED-FCS to solutions discussed hereby offers a decrease of the observed volume and time scale by up to an order of magnitude. Further reduction of these parameters is precluded by the out-of-focus broadening of p_{eff}. This phenomenon causes apparent lengthening of diffusion times and increase in the probe number (when compared to values expected on the basis of experiments in 2D systems). Application of the proposed data analysis methodology allows us to reproduce the correct probe number and effective dimension of the detection volume. Importantly, the procedure is based on the $P_{\mathrm{STED}}/P_{\mathrm{sat}}$ ratio, which is extracted from the data recorded during the actual STED-FCS experiment. It should prove invaluable for anomalous diffusion [12,37] studies (to control the investigated length scale) as well as for FCS measurements at high probe concentrations and kinetic investigations of fast processes [38]. Crucially, STED-FCS opens new perspectives for biophysical and biochemical studies [1,10,17,39,40], allowing us to precisely localize the measurement spot in a cell/organelle, vary the length scale of observation, and study the molecular dynamics *in vivo*. The approach we describe hereby not only grants straightforward data interpretation but also allows us to elude the errors related to direct application of the ω_{eff} values obtained in standard calibration procedures (which often do not match the actual conditions of a biological experiment). Therefore, we believe that it will prove particularly useful for *in vivo* studies utilizing STED-FCS.

The model we propose is also applicable to the emerging modifications of STED microscopy such as STEDD [27] or SPLIT [17]. Decrease in τ_D beyond the limits we establish can be realized by two-photon excitation [41] or, ultimately, adding another STED mode to trim the z dimension of the detection volume. Although technically possible [11,16], this is much more complex experimentally and would require an accurate description of the effective detection profile and its implementation in the autocorrelation integrals.

Funding. Narodowe Centrum Nauki (NCN) (UMO-2016/22/A/ST4/00017).

Acknowledgment. We thank Felix Koberling (PicoQuant) for critical reading of this paper as well as Marta Janczuk-Richter and Joanna Niedziolka-Jonsson (IPC PAS) for enabling us with UV–Vis spectroscopy measurements. We are grateful to Maciej Wojtkowski (IPS PAS), holder of the Horizon 2020 ERA CHAIR, for inspiring discussions.

See Supplement 1 for supporting content.

REFERENCES AND NOTES

1. B. Huang, H. Babcock, and X. Zhuang, "Breaking the diffraction barrier: super-resolution imaging of cells," Cell **143**, 1047–1058 (2010).
2. V. Westphal and S. W. Hell, "Nanoscale resolution in the focal plane of an optical microscope," Phys. Rev. Lett. **94**, 143903 (2005).
3. M. J. Rust, M. Bates, and X. Zhuang, "Sub-diffraction-limit imaging by stochastic optical reconstruction microscopy (STORM)," Nat. Methods **3**, 793–796 (2006).
4. S. T. Hess, T. P. Girirajan, and M. D. Mason, "Ultra-high resolution imaging by fluorescence photoactivation localization microscopy," Biophys. J. **91**, 4258–4272 (2006).

5. B. Harke, J. Keller, C. K. Ullal, V. Westphal, A. Schonle, and S. W. Hell, "Resolution scaling in STED microscopy," Opt. Express **16**, 4154–4162 (2008).
6. F. Göttfert, C. A. Wurm, V. Mueller, S. Berning, V. C. Cordes, A. Honigmann, and S. W. Hell, "Coaligned dual-channel STED nanoscopy and molecular diffusion analysis at 20 nm resolution," Biophys. J. **105**, L01–L03 (2013).
7. E. Rittweger, K. Y. Han, S. E. Irvine, C. Eggeling, and S. W. Hell, "STED microscopy reveals crystal color centres with nanometric resolution," Nat. Photonics **3**, 144–147 (2009).
8. S. W. Hell and J. Wichmann, "Breaking the diffraction resolution limit by stimulated emission: stimulated-emission-depletion fluorescence microscopy," Opt. Lett. **19**, 780–782 (1994).
9. T. A. Klar and S. W. Hell, "Subdiffraction resolution in far-field fluorescence microscopy," Opt. Lett. **24**, 954–956 (1999).
10. T. Müller, C. Schumann, and A. Kraegeloh, "STED microscopy and its applications: new insights into cellular processes on the nanoscale," Chem. Phys. Chem. **13**, 1986–2000 (2012).
11. L. Kastrup, H. Blom, C. Eggeling, and S. W. Hell, "Fluorescence fluctuation spectroscopy in subdiffraction focal volumes," Phys. Rev. Lett. **94**, 178104 (2005).
12. C. Eggeling, C. Ringemann, R. Medda, G. Schwarzmann, K. Sandhoff, S. Polyakova, V. N. Belov, B. Hein, C. von Middendorff, A. Schonle, and S. W. Hell, "Direct observation of the nanoscale dynamics of membrane lipids in a living cell," Nature **457**, 1159–1162 (2009).
13. M. P. Clausen, E. Sezgin, J. B. de la Serna, D. Waithe, B. C. Lagerholm, and C. Eggeling, "A straightforward approach for gated STED-FCS to investigate lipid membrane dynamics," Methods **88**, 67–75 (2015).
14. G. Vicidomini, H. Ta, A. Honigmann, V. Mueller, M. P. Clausen, D. Waithe, S. Galiani, E. Sezgin, A. Diaspro, and S. W. Hell, "STED-FLCS: an advanced tool to reveal spatiotemporal heterogeneity of molecular membrane dynamics," Nano Lett. **15**, 5912–5918 (2015).
15. M. Koenig, P. Reisch, R. Dowler, B. Kraemer, S. Tannert, M. Patting, M. P. Clausen, S. Galiani, C. Eggeling, F. Koberling, and R. Erdmann, "ns-time resolution for multispecies STED-FLIM and artifact free STED-FCS," Proc. SPIE **9712**, 97120T (2016).
16. C. Ringemann, B. Harke, C. Von Middendorff, R. Medda, A. Honigmann, R. Wagner, M. Leutenegger, A. Schonle, S. W. Hell, and C. Eggeling, "Exploring single-molecule dynamics with fluorescence nanoscopy," New J. Phys. **11**(10), 103054 (2009).
17. L. Lanzano, L. Scipioni, M. Di Bona, P. Bianchini, R. Bizzarri, F. Cardarelli, A. Diaspro, and G. Vicidomini, "Measurement of nanoscale three-dimensional diffusion in the interior of living cells by STED-FCS," Nat. Commun. **8**, 65 (2017).
18. T. Kalwarczyk, K. Sozanski, A. Ochab-Marcinek, J. Szymanski, M. Tabaka, S. Hou, and R. Holyst, "Motion of nanoprobes in complex liquids within the framework of the length-scale dependent viscosity model," Adv. Colloid Interface Sci. **223**, 55–63 (2015).
19. O. Krichevsky and G. Bonnet, "Fluorescence correlation spectroscopy: the technique and its applications," Rep. Prog. Phys. **65**, 251–297 (2002).
20. J. Lakowicz, *Principles of Fluorescence Spectroscopy* (Springer, 2006).
21. Due to the symmetry of the system, we use throughout the whole article cylindrical coordinates with the origin at the intersection of the optical axis and the focal plane, so that $\mathbf{r} = (r, z)$.
22. P. Kapusta, M. Wahl, and R. Erdmann, *Advanced Photon Counting*, Vol. 15 of Springer Series on Fluorescence (Springer, 2015).
23. We denote by "radius" the distance between the center of a Gaussian and the point where its normalized intensity drops to $1/e^2$.
24. D. E. Koppel, "Statistical accuracy in fluorescence correlation spectroscopy," Phys. Rev. A **10**, 1938–1945 (1974).
25. S. T. Hess and W. W. Webb, "Focal volume optics and experimental artifacts in confocal fluorescence correlation spectroscopy," Biophys. J. **83**, 2300–2317 (2002).
26. P. Kask, C. Eggeling, K. Palo, U. Mets, M. Cole, and K. Gall, "Fluorescence intensity distribution analysis (FIDA) and related fluorescence fluctuation techniques: theory and practice," in *Fluorescence Spectroscopy, Imaging and Probes: New Tools in Chemical, Physical and Life Sciences*, R. Kraayenhof, A. J. Visser, and H. Gerritsen, eds. (Springer, 2002), Chap. 9, pp. 152–181.
27. P. Gao, B. Prunsche, L. Zhou, K. Nienhaus, and G. U. Nienhaus, "Background suppression in fluorescence nanoscopy with stimulated emission double depletion," Nat. Photonics **11**, 163–169 (2017).
28. M. Reuss, J. Engelhardt, and S. W. Hell, "Birefringent device converts a standard scanning microscope into a STED microscope that also maps molecular orientation," Opt. Express **18**, 1049–1058 (2010).
29. M. Reuss, "Simpler STED Setups," Ph.D. thesis (Ruperto-Carola University of Heidelberg, 2010).
30. T. Schonau, T. Siebert, R. Hartel, T. Eckhardt, D. Klemme, K. Lauritsen, and R. Erdmann, "Pulsed picosecond 766 nm laser source operating between 1–80 MHz with automatic pump power management," Proc. SPIE **8604**, 860409 (2013).
31. G. Vicidomini, G. Moneron, K. Y. Han, V. Westphal, H. Ta, M. Reuss, J. Engelhardt, C. Eggeling, and S. W. Hell, "Sharper low-power STED nanoscopy by time gating," Nat. Methods **8**, 571–573 (2011).
32. J. R. Moffitt, C. Osseforth, and J. Michaelis, "Time-gating improves the spatial resolution of STED microscopy," Opt. Express **19**, 4242–4254 (2011).
33. G. Vicidomini, A. Schonle, H. Ta, K. Y. Han, G. Moneron, C. Eggeling, and S. W. Hell, "STED nanoscopy with time-gated detection: theoretical and experimental aspects," PLoS ONE **8**, e54421 (2013).
34. M. Dyba, J. Keller, and S. Hell, "Phase filter enhanced STED-4pi fluorescence microscopy: theory and experiment," New J. Phys. **7**(1), 134 (2005).
35. P. Torok and P. Munro, "The use of Gauss–Laguerre vector beams in STED microscopy," Opt. Express **12**, 3605–3617 (2004).
36. C. Tressler, M. Stolle, and C. Fradin, "Fluorescence correlation spectroscopy with a doughnut-shaped excitation profile as a characterization tool in STED microscopy," Opt. Express **22**, 31154–31166 (2014).
37. D. S. Banks, C. Tressler, R. D. Peters, F. Hofling, and C. Fradin, "Characterizing anomalous diffusion in crowded polymer solutions and gels over five decades in time with variable-lengthscale fluorescence correlation spectroscopy," Soft Matter **12**, 4190–4203 (2016).
38. X. Zhang, A. Poniewierski, A. Jelinska, A. Zagozdzon, A. Wisniewska, S. Hou, and R. Holyst, "Determination of equilibrium and rate constants for complex formation by fluorescence correlation spectroscopy supplemented by dynamic light scattering and Taylor dispersion analysis," Soft Matter **12**, 8186–8194 (2016).
39. C. Eggeling, K. I. Willig, and F. J. Barrantes, "STED microscopy of living cells-new frontiers in membrane and neurobiology," J. Neurochem. **126**, 203–212 (2013).
40. T. Niehorster, A. Loschberger, I. Gregor, B. Kramer, H.-J. Rahn, M. Patting, F. Koberling, J. Enderlein, and M. Sauer, "Multi-target spectrally resolved fluorescence lifetime imaging microscopy," Nat. Methods **13**, 257–262 (2016).
41. J. T. King, C. Yu, W. L. Wilson, and S. Granick, "Super-resolution study of polymer mobility fluctuations near c*," ACS Nano **8**, 8802–8809 (2014).